

# Quantitative characterization of the focusing process and dynamic behavior of differently sized microparticles in a spiral microchannel

Nan Xiang · Ke Chen · Dongke Sun ·  
Shanfang Wang · Hong Yi · Zhonghua Ni

Received: 25 April 2012 / Accepted: 27 June 2012 / Published online: 8 July 2012  
© Springer-Verlag 2012

**Abstract** In this paper, a spiral microchannel was fabricated to systematically investigate particle dynamics. The focusing process or migration behavior of different-sized particles in the outlet region was presented. Specifically, for focused microparticles, quantitative characterization and analysis of how particles migrate towards the equilibrium positions with the increase in flow rate ( $De = 0.31–3.36$ ) were performed. For unfocused microparticles, the particle migration behavior and the particle-free region's formation process were characterized over a wide range of flow rates ( $De = 0.31–4.58$ ), and the emergence of double particle-free regions was observed at  $De \geq 3.36$ . These results provide insights into the design and operation of high-throughput particle/cell filtration and separation. Furthermore, using the location markers prefabricated along with the microchannel structures, the focusing or migration dynamics of different-sized particles along the spiral microchannel was systematically explored. The particle migration length effects on focusing degree and particle-free region width were analyzed. These analyses may be valuable for the optimization of microchannel structures. In addition, this device was successfully used to efficiently filter rare particles from a large-volume sample and separate particles of two different sizes according to their focusing states.

**Keywords** Inertial effects · Spiral microchannel · Dynamic behavior · Focusing process · Quantitative characterization

## 1 Introduction

Efficient and precise manipulation of microparticles or cells/macromolecules can be achieved by utilizing inertial effects in microfluidics. Inertial microfluidics has many advantages such as high-throughput processing in a continuous mode, simple planar structure for easy fabrication, non-invasive manipulation without complex label, and convenient operation without external fields. In the past several years, various prototype devices have been developed to realize important functions such as particle/cell focusing (Russom et al. 2009; Xuan et al. 2010; Choi et al. 2011), trapping (Mach et al. 2011), separation (Di Carlo et al. 2007; Yoon et al. 2009; Lee et al. 2011), transportation (Kim and Yoo 2008), filtration (Seo et al. 2007a; Bhagat et al. 2008b), encapsulation (Edd et al. 2008) and biochemical reagent mixing (Sudarsan and Ugaz 2006a, b). In addition to simple straight channels (Bhagat et al. 2009; Choi et al. 2011), other microchannel configurations, including single curves (Yoon et al. 2009), symmetric or asymmetric sinusoidal lines (Di Carlo et al. 2007), contraction–expansion arrays (Lee et al. 2011; Sim et al. 2011), and spirals (Sudarsan and Ugaz 2006a; Seo et al. 2007a, b; Kuntaegowdanahalli et al. 2009) have been adopted. The spiral microchannels (Sudarsan and Ugaz 2006a; Seo et al. 2007a, b; Bhagat et al. 2008a; Russom et al. 2009; Kuntaegowdanahalli et al. 2009; Wang et al. 2010), in particular, attract significant attention because strong Dean flow can be maintained for extended period in a compact manner.

N. Xiang · K. Chen · D. Sun · S. Wang · H. Yi · Z. Ni (✉)  
School of Mechanical Engineering, Southeast University,  
Nanjing 211189, People's Republic of China  
e-mail: nzh2003@seu.edu.cn

N. Xiang · K. Chen · D. Sun · S. Wang · H. Yi · Z. Ni  
Jiangsu Key Laboratory for Design and Manufacture  
of Micro-Nano Biomedical Instruments, Southeast University,  
Nanjing 211189, People's Republic of China

For example, the Dean flow induced in spiral microchannels has been used to enhance mixing (Sudarsan and Ugaz 2006a) and to rotate cells in electroporation systems for efficient gene delivery (Wang et al. 2010). Precise particle/cell manipulation can be realized by coupling the inertial migration and Dean flow. Russom et al. (2009), for instance, fabricated a spiral microchannel with gradually varied width to keep the lateral displacements of particles constant. In addition, they plotted a useful focusing state spectrum to guide the designing of these devices. Bhagat et al. (2010) developed a sheathless microflow cytometer by integrating an inertial focusing unit with a laser induced fluorescence (LIF) set-up, which could achieve a high throughput up to  $\sim 2,100$  particles per second. Realizing that the particle/cell focusing is size dependent in the spiral microchannels, passive separation and filtration of different size particles/cells have been demonstrated. For example, Bhagat et al. (2008a) observed different focusing states between  $7.32$  and  $1.9 \mu\text{m}$  particles at the same flow rate, based on which they achieved high-throughput separation of these two particles. Kuntaegowdanahalli et al. (2009) demonstrated a scheme for complete separation of multi-sized particles/cells by exploiting the effects of the channel dimension, particle size and flow rate on equilibrium positions of focused particles. Seo et al. (2007a, b) developed a membrane-free microseparator with a double-spiral design for effective filtering or sorting microparticles. They also studied the transverse motion of particles near the center junction and the effect of flow rate on separation.

In the above-mentioned studies, efforts have been made to characterize and understand the dynamic behavior of particles in spiral microchannels. However, systematic studies disclosing detailed information of particle dynamics are still lacking. For example, most reports focus on the behavior of those particles that are well focused in the outlet region, with little attention being paid to the particle behavior during the focusing process (i.e., how particles gradually move towards the equilibrium positions with the increase in flow rate). In addition, detailed investigations on the migration behavior of unfocused particles (particles that are not focused at any flow rate) in the outlet region are also scarce. Quantitative characterization and analysis of these rarely studied behaviors, however, can provide insights into the device design and the best operation protocol. Moreover, quantitative investigation of the focusing or migration behavior of different-sized particles at specific locations along the spiral microchannel may be helpful for optimizing microchannel structures but has not been systematically reported so far.

In this work, a miniaturized microfluidic device with a planar Archimedean spiral microchannel (Fig. 1) was designed and fabricated to systematically investigate particle dynamics. The focusing process or dynamic behavior of the differently sized microparticles distributed in the

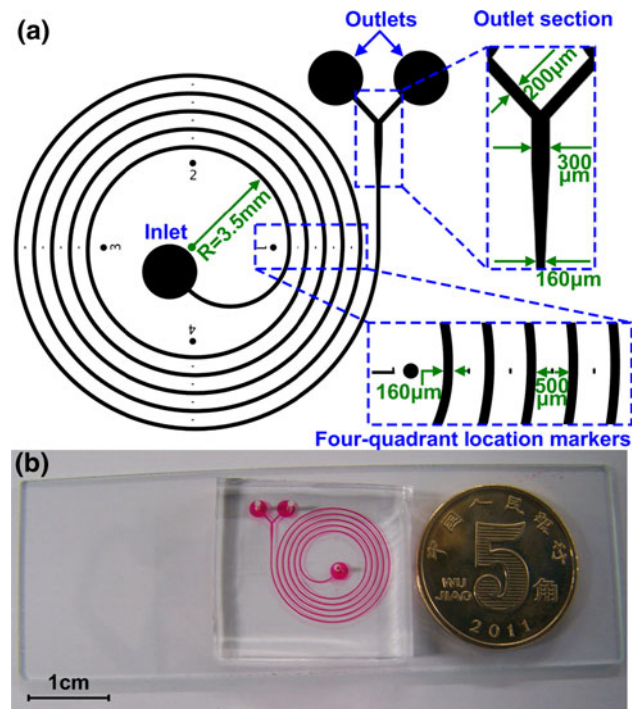


**Fig. 1** Detailed structure and dimension of the microfluidic device with a spiral microchannel. **a** Reversed monochrome photo-mask used in the photolithography process. Partial enlargements of the image show detailed structures of the four-quadrant location markers and the outlet section. **b** Photograph of the fabricated PDMS microfluidic device with a five-loop spiral microchannel (the microchannel is fully filled with red ink for visualization). The scale bar is 1 cm

microchannel outlet region was characterized and analyzed through fluorescent stream images and intensity spectrums. The particle stream width and position (for  $4.8 \mu\text{m}$  focused particles), and the particle-free region width (for  $2.1 \mu\text{m}$  unfocused particles) were quantitatively measured. Several new phenomena were observed, such as the shift direction and non-uniform intensity distribution of particle streams and the emergence of double particle-free regions, and then, possible explanations were provided. Moreover, the focusing or migration dynamics of microparticles along the spiral microchannel was investigated by using the pre-fabricated location markers. The effects of migration length on particle focusing degree or particle-free region width were also analyzed. Finally, based on the analysis of particle migration behavior, this device was successfully used to efficiently filter rare particles and separate particles of two different sizes according to their specific focusing states.

## 2 Basic theory and design principle

Physical phenomena of fluid and particle behavior flowing through microfluidic channels can be analyzed by using

dimensionless numbers. Reynolds number ( $Re$ ), one of the important dimensionless numbers which is defined as the ratio of inertial force to viscous force, is extremely low in microfluidic devices ( $Re = 10^{-6} \sim 10$ ) under general conditions (Squires and Quake 2005). However, when the channel Reynolds number is finite, the particle flowing through a spiral microchannel will be influenced by both inertial migration effect and Dean flow (Bhagat et al. 2008a; Kuntaegowdanahalli et al. 2009; Russom et al. 2009).

When the inertial migration of particles occurs, the microparticle experiences a drag force along the main flow direction as well as an inertial lift force ( $F_L$ ) perpendicular to this direction. The inertial lift force ( $F_L$ ) which drives particles to migrate towards the equilibrium positions is actually the net force of a shear-induced inertial lift force ( $F_{LS}$ ) directed to the microchannel wall and a wall-induced inertial lift force ( $F_{LW}$ ) to the microchannel center. The magnitudes of these two forces are dependent on the particle position in the microchannel cross-section, with the shear-induced lift force ( $F_{LS}$ ) dominating in the center region and the wall-induced inertial lift force ( $F_{LW}$ ) dominating in the wall region (Di Carlo et al. 2007; Bhagat et al. 2009). Expression for the net lift force can be written as (Asmolov 1999; Choi and Lee 2010):

$$F_L = \frac{\rho U_m^2 a_p^4 C_L}{D_h^2} \quad (1)$$

where,  $\rho$  is the density of fluid,  $U_m$  is the maximum fluid velocity which can be estimated as  $2 \times U_f$  ( $U_f$  denoting the average fluid velocity),  $a_p$  is the diameter of microparticle,  $C_L$  is the dimensionless lift coefficient whose value and sign are determined by the channel Reynolds number and particle position in the microchannel,  $D_h$  is the microchannel hydraulic diameter which can be approximated as  $2WH/(W+H)$  for the rectangular cross-section microchannel ( $W$  and  $H$  denoting the microchannel width and height, respectively). An estimate of this net lift force can be made by using an average value of  $C_L \sim 0.5$  (Di Carlo et al. 2007; Bhagat et al. 2008a).

Due to the presence of Dean flow in the spiral microchannel, particle is also subjected to a Dean drag force which entrains it to follow the fluid movement within two symmetric Dean vortices located, respectively, in the top and bottom half of the microchannel. The strength of transverse Dean flow is positively related to the value of a dimensionless number called Dean number ( $De$ ), demonstrated by Berger et al. (1983)

$$De = Re \sqrt{\frac{D_h}{2R}} = \frac{\rho U_f D_h}{\eta} \sqrt{\frac{D_h}{2R}} \quad (2)$$

where  $R$  is the radius of spiral microchannel, and  $\eta$  is the dynamic viscosity. With the Dean drag force and the Dean

velocity being in a consistent direction, the magnitude of this force can be approximated by assuming the Stokes drag (Bhagat et al. 2008a):

$$F_D = 3\pi\eta a_p \bar{U}_D \quad (3)$$

Here,  $\bar{U}_D$  is the average Dean velocity which scales as  $\bar{U}_D = 1.8 \times 10^{-4} De^{1.63}$  offered by Ookawara et al. (2004) through numerical simulation. The presence of Dean drag force makes the equilibrium position and motion of particle in spiral microchannels more complex than those in straight microchannels. Within a low-aspect-ratio spiral microchannel, randomly dispersed particles near the inlet will move towards the two equilibrium positions along the channel height while they are migrating to the outlets. Additionally, in order to make all particles focused, the dimensions of particle and channel should satisfy  $a_p/L_c \geq 0.07$  (where,  $L_c$  is the characteristic length of the microchannel cross-section. For low-aspect-ratio microchannels, it can be replaced by the microchannel height) (Bhagat et al. 2008a; Di Carlo et al. 2007).

### 3 Materials and methods

#### 3.1 Device design and fabrication

The spiral microchannel used in this work consists of five-loop channels with one inlet and two outlets. The main microchannel structure is  $160 \mu\text{m}$  wide with spacing between two adjacent loops fixed at  $500 \mu\text{m}$  and an initial radius of the spiral at  $3.5 \text{ mm}$ . In the outlet region, the microchannel gradually expands to  $300 \mu\text{m}$  wide, and then bifurcates into two outlets. The detailed structure and dimension of the spiral microchannel are shown in Fig. 1a. In order to characterize the focusing or migration behavior of fluorescent particles at different locations along the spiral microchannel, four-quadrant location markers ( $0^\circ$ ,  $90^\circ$ ,  $180^\circ$  and  $270^\circ$ ) were pre-fabricated together with the microchannel structures (Fig. 1a). The total length of the spiral microchannel is  $\sim 16 \text{ cm}$ . The device used in this work was designed and drawn in the AutoCAD 2010 (AutoDesk, Inc.) and converted to monochrome BMP format photo-mask ( $13,680 \times 11,120$  pixels, with a pixel size of  $1.25 \mu\text{m}$ ) by plotting function of CAD software. After being sliced into small parts in the height direction, the photo-masks were loaded for exposure in a maskless lithography system SF-100 Xtreme (Intelligent Micro Patterning, LLC), and then an SU-8 master of  $\sim 50 \mu\text{m}$  thick was fabricated using standard photolithography technique. Using this master mold, PDMS molding was carried out to replicate the microstructure features. After being cured, the PDMS chip was peeled from the master,

and the inlet and outlets reservoirs were punched using a Harris Uni-Core biopsy micropunch (0.75 mm, Electron Microscopy Sciences). Finally, the PDMS chip was permanently bonded to a clean glass slide through UV/Ozone treatment (144AX-220, JELIGHT COMPANY, Inc.). The photograph of the final device is shown in Fig. 1b. The overall size of the microchannel region is  $\sim 2 \text{ cm}^2$ .

### 3.2 Preparation of particle suspensions

Aqueous fluorescent polystyrene microparticles with sizes of 4.8 and 2.1  $\mu\text{m}$  (Thermo Fisher Scientific, Inc.) were used as manipulation objects for focusing, filtration, and separation. The concentration and specific gravity of initial particle suspensions were 1 % solids and  $1.06 \text{ g/cm}^3$ , respectively. The testing particle suspensions were prepared in 0.5 wt% Tween 20 (Sigma-Aldrich) aqueous solutions to reduce the chances of particle aggregation. The final concentration of testing particle suspensions was only  $\sim 0.015 \%$  (v/v) so that the interparticle interactions can be neglected. In addition, their dynamic viscosity useful for calculating the Dean number was  $\sim 1.084 \times 10^{-3} \text{ kg m}^{-1} \text{ s}^{-1}$ . Additionally, due to the unique property of spiral microchannels that radii vary with loops, the Dean number used in this work was calculated with the initial radius unless special notice is given.

### 3.3 Experimental set-up and operation

PEEK tubing (1569, Upchurch Scientific) was used to connect the inlet port with a 3 ml plastic syringe (78-0851, KD Scientific, Inc.) by a 25 G luer stub adapter (5225-B, AXXON). After the testing particle suspensions being loaded, the syringe was mounted onto a programmable syringe pump (KDS201, KD Scientific, Inc.). During the experimental testing, the whole device was fixed on the stage of an inverted fluorescence microscope (IX71, Olympus). A 120 W fluorescence illumination system (X-Cite 120, EXFO) was used as an excitation light source. Two differently fluorescent-labeled microparticles were visualized through a  $10\times$  objective (UPLFLN,  $10\times/0.3$ ) and two fluorescence mirror units (U-MWU2, U-MWB2). High-speed particle motions were recorded using a 14-bit camera (Exi Blue, Qimaging) and the IMAGE-PRO EXPRESS software (Media Cybernetics, Inc.).

### 3.4 Image processing and analyzing

In order to quantitatively characterize and analyze high-speed particle motions, over 100 images were continuously captured at the same location with an exposure time of 500 ms. Then, the IMAGEJ software (version 1.45s, NIH, USA) was used as an image post-processing tool to overlay

and normalize each pixel value in the obtained images. Due to the dark background under the fluorescence illumination condition, a bright-field image of the microchannel captured at the same position was stacked with the obtained composite images (using ‘Images to Stack’ option of IMAGEJ software) to precisely determine the walls of the microchannel. At the same time, grayscale values across the width of the microchannel were also measured using this software so that the distribution and behavior of the microparticles can be accurately characterized and analyzed without using any ultra-speed camera. Moreover, all the experimental images were captured at the bottom of the microchannel wall. Therefore, experimental results at different flow rates or locations can be compared.

## 4 Results and discussion

### 4.1 Focusing process of 4.8 $\mu\text{m}$ particles in the outlet region

The fluorescent stream images illustrating the distribution of 4.8  $\mu\text{m}$  fluorescent polystyrene microparticles in the outlet (just before the expanding section) and inlet regions of the spiral microchannel at low Reynolds numbers ( $Re < 33$ ) are shown in Fig. 2. In the inlet region (Fig. 2a), particles are randomly dispersed across the microchannel width at a relatively high flow rate ( $De = 2.75$ ). In the outlet region, however, particles begin to migrate towards the equilibrium positions near the inner microchannel wall at  $De = 0.31$  and particle-free regions are observed near inner and outer walls (Fig. 2b). With  $De$  increasing from 0.31 to 3.36, an increasing number of particles intend to migrate towards the equilibrium positions (Fig. 2b–g).

Figure 3 shows the normalized fluorescent intensity distribution of 4.8  $\mu\text{m}$  particle streams across the microchannel’s outlet width during the whole focusing process ( $De = 0.31$ – $3.36$ ). In order to better understand it, the focusing process is artificially divided into two stages. At the first stage ( $De = 0.31$ – $1.53$ ), as is shown in Fig. 3a, the transverse migration of 4.8  $\mu\text{m}$  particles is observed to occur as a result of the interference of inertial lift force and Dean drag force. However, neither of these two forces whose magnitudes are proportional to the average flow rate of fluid  $F_L \propto U_f^2$ ,  $F_D \propto U_f^{1.63}$  (Bhagat et al. 2008a; Kuntaegowdanahalli et al. 2009) are strong enough to drive all the particles towards the equilibrium positions within this flow rate range, causing that particle streams remain relatively wide. Additionally, intensities of fluorescent streams at flow rates of this range are non-uniformly distributed, with the peaks of normalized fluorescent intensity curves emerging at similar positions in the inner half of



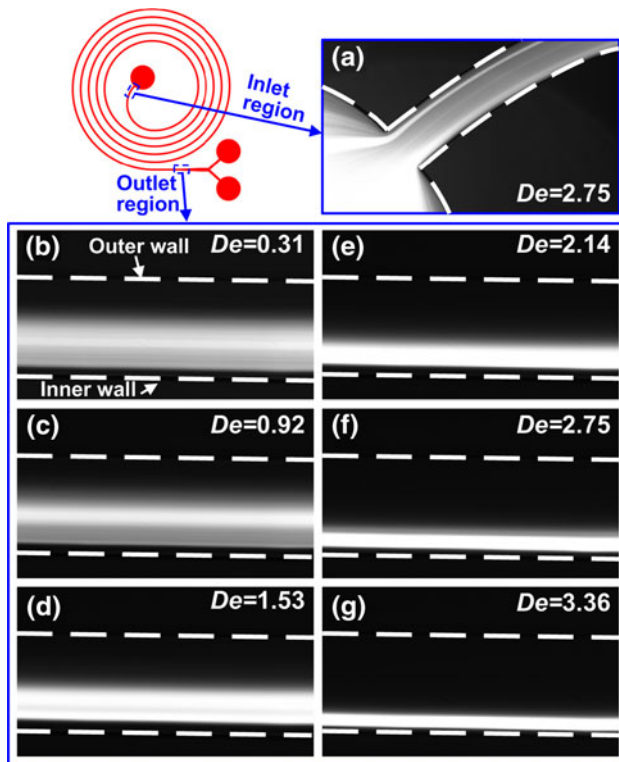


**Fig. 2** Fluorescent stream images illustrating the distribution of 4.8 μm microparticles near the microchannel inlet and outlet regions at low Reynolds numbers. **a**  $De = 2.75$  near the inlet region. **b–g**  $De = 0.31–3.36$  near the outlet region. White dotted lines in the figures indicate the microchannel walls

microchannel. This is because although the weakness of inertial lift force and Dean drag force causes that all particles cannot be well focused in the limited microchannel length (~16 cm) used in this work, a certain number of particles which are initially located close to the equilibrium positions have already focused in these positions, which are manifested by the peaks of fluorescent intensity curves. As the flow rate increases to  $De = 1.53$ , most of the non-equilibrium particles have transversely migrated near the equilibrium positions so that the intensities across fluorescent streams appear to be uniform (Fig. 2d–g). The second stage of focusing process ( $De = 1.83–3.36$ ) is shown in Fig. 3b, where it is clearly observed that with increasing flow rate the focusing degree increases (or the width of fluorescent streams decreases). At the same time, the position of the fluorescent stream in the microchannel gradually moves towards the inner wall with increasing flow rate. This finding is different from that demonstrated by Kuntaegowdanahalli et al. (2009), who found that the well-focused particle stream moved away from the microchannel wall with increasing flow rate. This difference may result from the variance in the dominant force subjected by microparticles. In our work, the microparticles

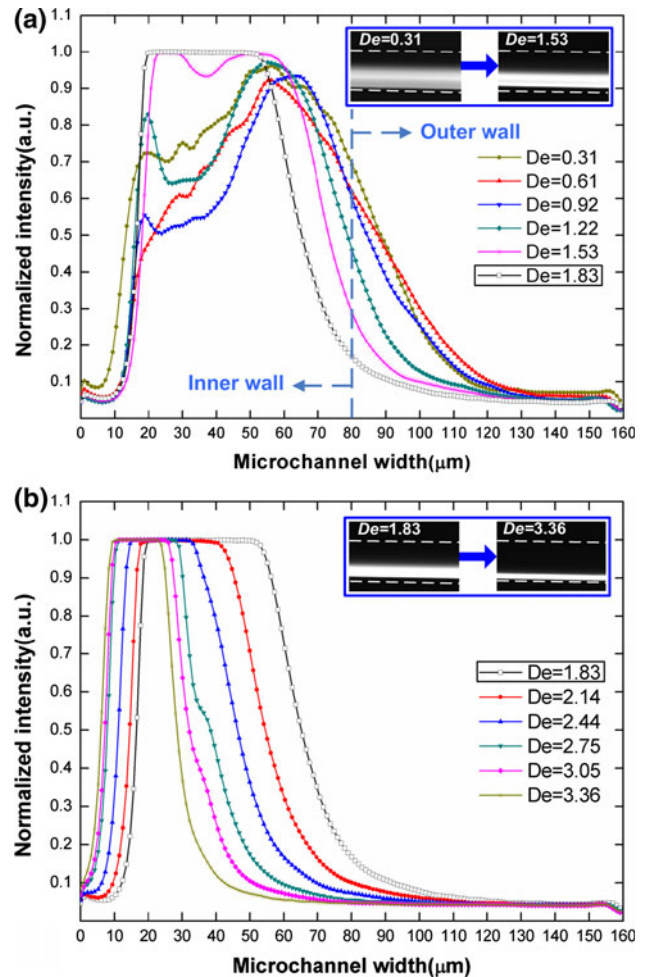


**Fig. 3** Normalized fluorescent intensity distributions of 4.8 μm particle streams across the microchannel outlets at low Reynolds numbers. **a** Normalized fluorescent intensity curves at  $De = 0.31–1.83$ . **b** Normalized fluorescent intensity curves at  $De = 1.83–3.36$ . The inset figures in figure **a** and **b** show the fluorescent stream images at minimum and maximum  $De$ . The curve at  $De = 1.83$  plotted both in figure **a** and **b** is used for comparison

are still in the focusing process when the Dean number is relatively small ( $De = 0.31–3.36$ ). The Dean drag force and inertial lift force calculated using Eqs. (1) and (3) indicate the dominance of inertial lift force for 4.8 μm particles at flow rates of this range ( $De < 3.36$ ). The inertial lift force will push the microparticles towards the inner wall. By comparison, their work focuses on the behavior of microparticles that have already occupied the equilibrium positions. They attribute their experimental finding to the fact that Dean drag force increases much faster than inertial lift force at higher levels of flow rates. The dominance of Dean drag force at much higher flow rates tested in their experiment moves the particles away from the inner microchannel wall.

In order to further investigate the focusing process of 4.8 μm particles and characterize the focusing degree of

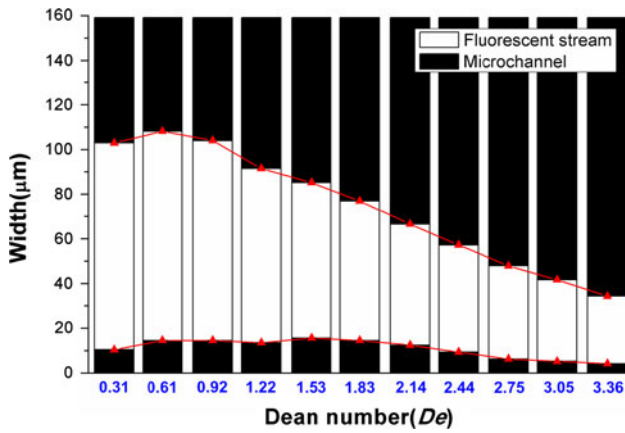


**Fig. 4** Width and position of 4.8 μm particle streams across the microchannel outlets at different  $De$ . The white columns represent the fluorescent streams and the black columns represent the microchannel (160 μm wide). The red curves illustrate the inner and outer boundaries of particle streams at varied  $De$

fluorescent streams at varied flow rates, the width and position of fluorescent streams relative to microchannel widths as a function of  $De$  are plotted in Fig. 4. As can be seen from this figure, the position and width of fluorescent streams in the microchannel remain constant until  $De$  increases to 1.22. After that, the width of fluorescent streams begins to decrease with increasing  $De$ , whereas the width of the particle-free regions near the outer wall shows an increasing trend, both indicating the increase of focusing degree. For the particle-free region near the inner wall, its width keeps almost unchanged up to  $De = 2.14$  before decreasing obviously. The width of the fluorescent stream at  $De = 3.36$  is much larger than the actual particle diameter (4.8 μm). Increasing the flow rate may further enhance the focusing effect.

**Fig. 5** Fluorescent stream images illustrating the distribution of 2.1 μm microparticles near the microchannel inlet and outlet regions at low Reynolds numbers. **a**  $De = 3.97$  near the inlet region. **b–i**  $De = 0.31–0.92$  and  $De = 3.36–4.58$  near the outlet region. White dotted lines in the figure indicate the microchannel walls. The formation process of the particle-free region near the outer microchannel wall is marked by red arrows in the figure **e–i**

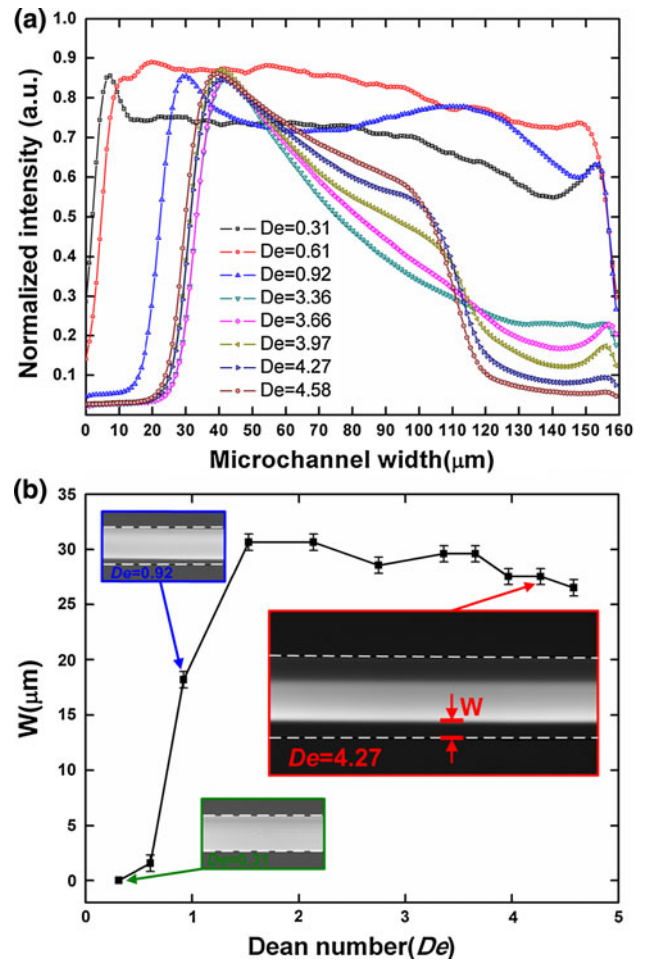
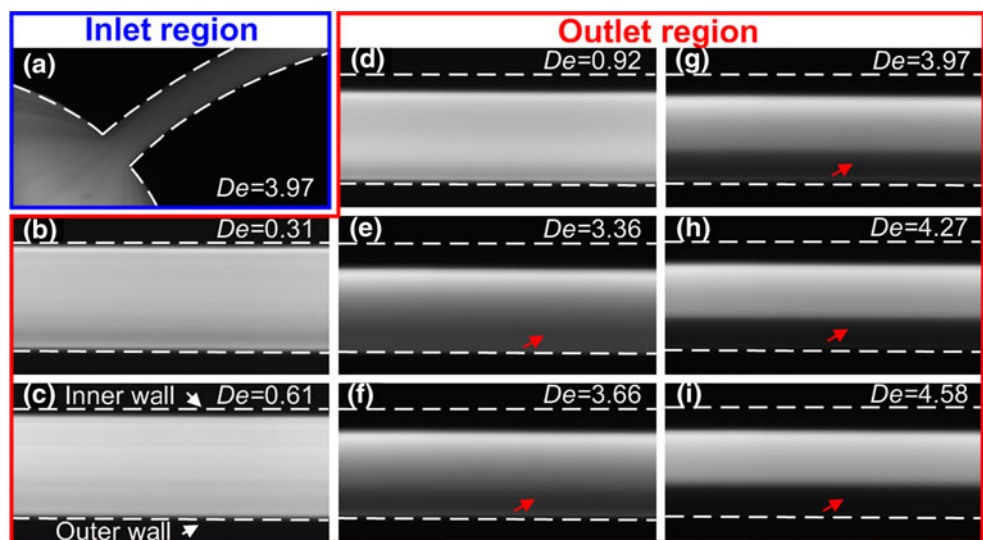
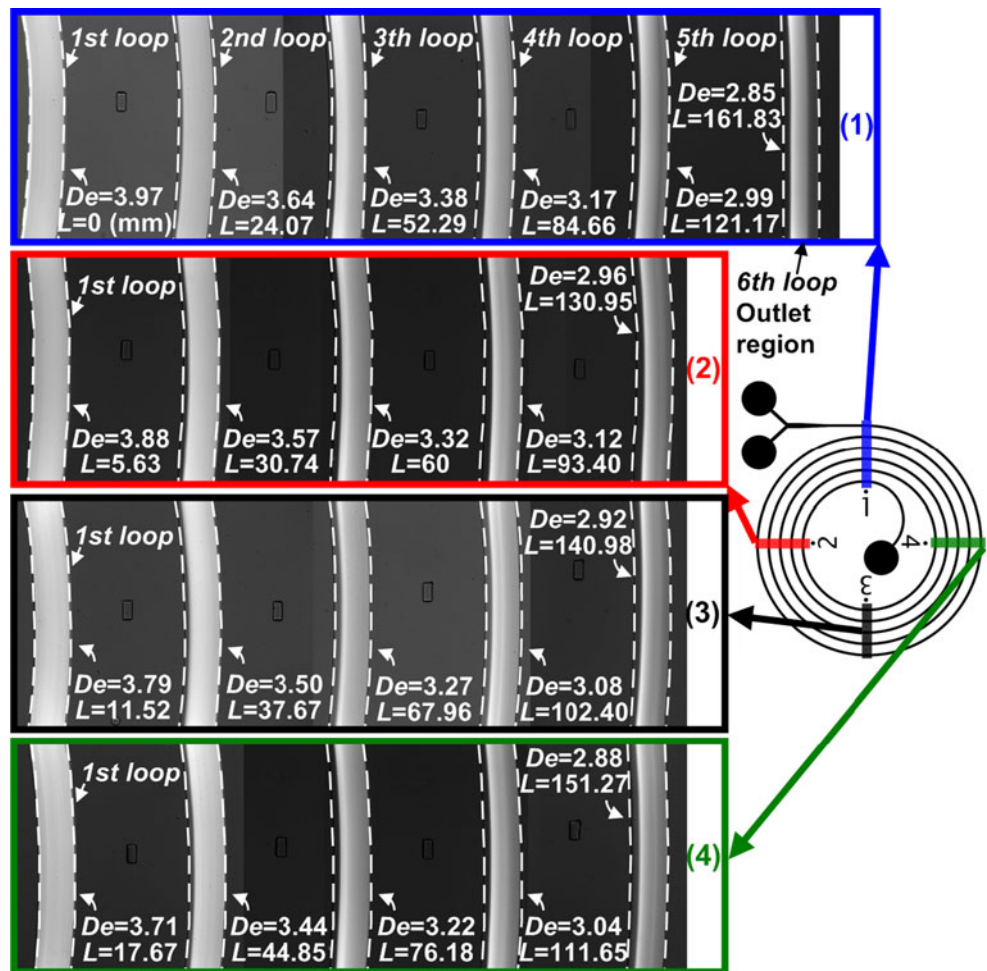


**Fig. 6** **a** Normalized fluorescent intensity distribution of 2.1 μm particles streams across the microchannel outlets at  $De = 0.31–0.92$  and  $De = 3.36–4.58$ . **b** Relationship between Dean number ( $De$ ) and width of the particle-free region near the inner wall ( $W$ ). The inset figures show the fluorescent stream images of 2.1 μm particles at  $De = 0.31, 0.92$  and  $4.27$

**Fig. 7** Fluorescent stream images of 2.1  $\mu\text{m}$  particles at  $De = 3.97$  captured near the marked locations (positions 1–4). White dotted lines in the figure indicate the microchannel walls. The detailed  $De$  and particle migration length ( $L$ ) at each marked location are illustrated, respectively



#### 4.2 Migration behavior of 2.1 $\mu\text{m}$ particles in the outlet region

Unlike 4.8  $\mu\text{m}$  particles ( $a_p/H \sim 0.1$ ) which are observed to be well focused near the inner wall of microchannel outlet at  $De = 3.36$ , 2.1  $\mu\text{m}$  particles behave in a completely different way. Since they do not satisfy the focusing condition ( $a_p/H \geq 0.07$ ), 2.1  $\mu\text{m}$  particles ( $a_p/H = 0.042$ ) will not focus towards the equilibrium positions or form a narrow stream at any flow rate. Understanding the migration behavior of these unfocused particles in spiral microchannels, however, will be of great value for achieving the separation of different-sized particles based on their focusing states.

Figure 5 shows the fluorescent stream images illustrating distribution of 2.1  $\mu\text{m}$  microparticles near the spiral microchannel inlet and outlet regions at low Reynolds numbers ( $Re < 45$ ). Figure 6a plots the normalized fluorescent intensity distribution of 2.1  $\mu\text{m}$  particles across the microchannel outlet. As shown in these two figures, 2.1  $\mu\text{m}$  particles are still randomly dispersed across the microchannel outlet at  $De = 0.31$  due to the weakness of inertial lift force and Dean drag force, whereas 4.8  $\mu\text{m}$  particles

have already moved towards the inner microchannel wall at the same flow rate (Fig. 2b). The fact accounting for this difference is that magnitudes of both inertial lift force and Dean drag force are proportional to the particle diameter, meaning that particles with larger diameters are subjected to greater force (Kuntaegowdanahalli et al. 2009; Bhagat et al. 2008a; Di Carlo et al. 2008). As the flow rate further increases to  $De \geq 0.61$ , a particle-free region is observed near the inner microchannel wall owing that the dominant Dean drag force moves particles towards the outer microchannel wall. This finding is in agreement with the experimental result reported by Bhagat et al. (2008a). The relationship between flow rate (Dean number) and width of the particle-free region near the inner wall is plotted in Fig. 6b. The width of particle-free regions increases rapidly as  $De$  increases from 0.31 to 1.53, and then remains constant at  $De > 1.53$ . After  $De$  increases to 3.36, a particle-free region is also found near the outer microchannel wall, the generating process of which is marked by red arrows in Fig. 5. The formation of double particle-free regions near the inner and outer microchannel walls in our experiment possibly results from the velocity difference in



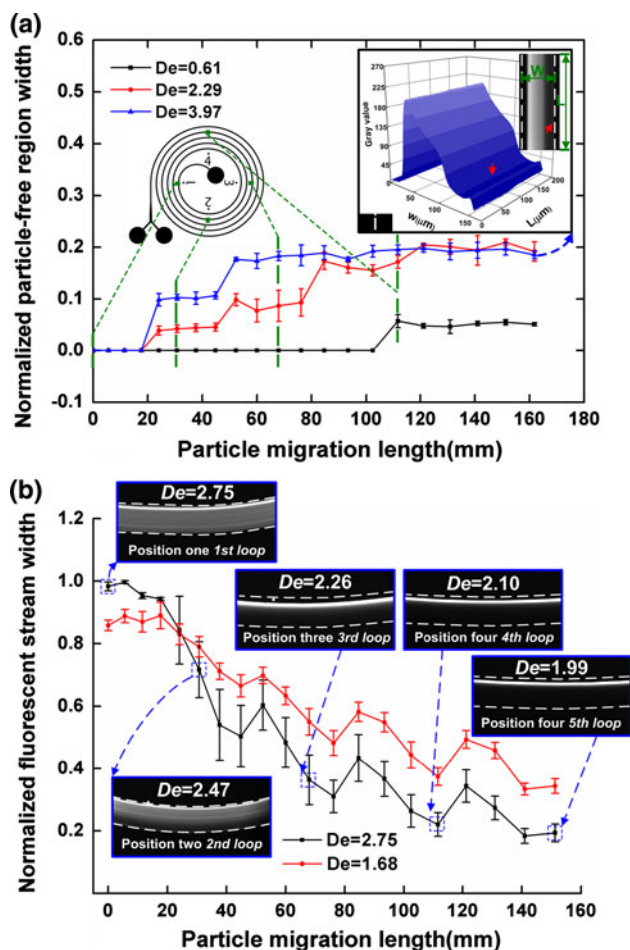


**Fig. 8** **a** Relationship between particle migration length and normalized particle-free region width of 2.1  $\mu\text{m}$  particles near the inner wall at three different flow rates. The inset figure **i** shows the three dimensional gray value distribution across the  $W \times L$  region near the outlet microchannel. Red arrows in this inset figure indicate the particle-free region near the outer wall. **b** Relationship between particle migration length and normalized fluorescent stream width of 4.8  $\mu\text{m}$  particles at two different flow rates ( $De = 2.75$  and 1.68). The inset photographs show the fluorescent stream images of 4.8  $\mu\text{m}$  particles captured near specific locations

Dean vortices. As noted in previous researches (Yoon et al. 2009; Gossett and Di Carlo 2009), the velocity directed outward is much larger than that directed inward or vertically, and the velocity directed inward shifts to intersect zero at a higher main flow rate, indicating that the drag force directed outward is much larger than that directed inward or vertically. Therefore, particles with their initial positions being near the inner wall will firstly be moved towards the outer wall at a relatively small flow rate, leading to the occurrence of a particle-free region near the inner wall. As the flow rate further increases, the drag forces directed inward and vertically turn to become strong enough to drive particles to migrate towards the inner wall from the top and bottom halves of the microchannel.

Hence, a particle-free region is gradually formed near the outer wall as shown in Fig. 5e–i.

#### 4.3 Dynamic behavior of 2.1 $\mu\text{m}$ particles along the spiral microchannel

Research on the dynamic behavior of different-sized particles at specific locations (loops) along the spiral microchannel will be potentially useful for the design and optimization of channel structures as well as the selection and optimization of experimental parameters. Given this goal, in this work, the dynamic behavior of 2.1  $\mu\text{m}$  particles under various flow rates at different locations ( $0^\circ$ ,  $90^\circ$ ,  $180^\circ$  and  $270^\circ$  four-quadrant locations in Fig. 1) along a spiral microchannel is characterized.

Figure 7 shows the fluorescent stream images of 2.1  $\mu\text{m}$  particles at  $De = 3.97$  captured near each location mark. It is worth mentioning that in the spiral microchannel the particle migration length ( $L$ ) along the main flow direction (the length of the spiral microchannel) increases and the Dean number ( $De$ ) decreases with increase in loops (radius of the microchannel). The detailed value of  $De$  and particle migration length ( $L$ ) at each marked locations are provided in Fig. 7. As can be seen from this figure, particles remain scattered across the microchannel at  $L \leq 17.67$  mm. However, when the particle migration length ( $L$ ) arrives at 24.07 mm, a particle-free region is observed near the inner wall, and then it gradually becomes wider with the length ( $L$ ) increases.

Curves describing the relationship between the particle migration length ( $L$ ) and the normalized particle-free region width at three different flow rates are shown in Fig. 8a. The shortest particle migration length for generating a particle-free region at  $De = 0.61$  ( $L \sim 102.4$  mm) is much larger than that at  $De = 2.29$  or 3.97 (both  $L \sim 17.67$  mm), indicating that at lower flow rate, much longer microchannel length is required for generating particle-free region of a certain width. The particle-free region width tends to be constant when particles migrate towards the outlets. After stabilizing, the widths of particle-free regions at  $De = 2.29$  and 3.97 show similar variation patterns with the latter region ( $De = 3.97$ ) being widened more rapidly. In contrast, the particle-free region at  $De = 0.61$  has much smaller width, which may be caused by the weakness of lateral forces experienced by the microparticles. More importantly, double particle-free regions appear only at  $De = 3.97$  and  $L \sim 161.83$  mm [Fig. 7 position (1) 6th loop and Fig. 8a inset figure i].

#### 4.4 Focusing dynamics of 4.8 $\mu\text{m}$ particles along the spiral microchannel

The inset photographs in Fig. 8b show the fluorescent stream images of 4.8  $\mu\text{m}$  particles at  $De = 2.75$  captured



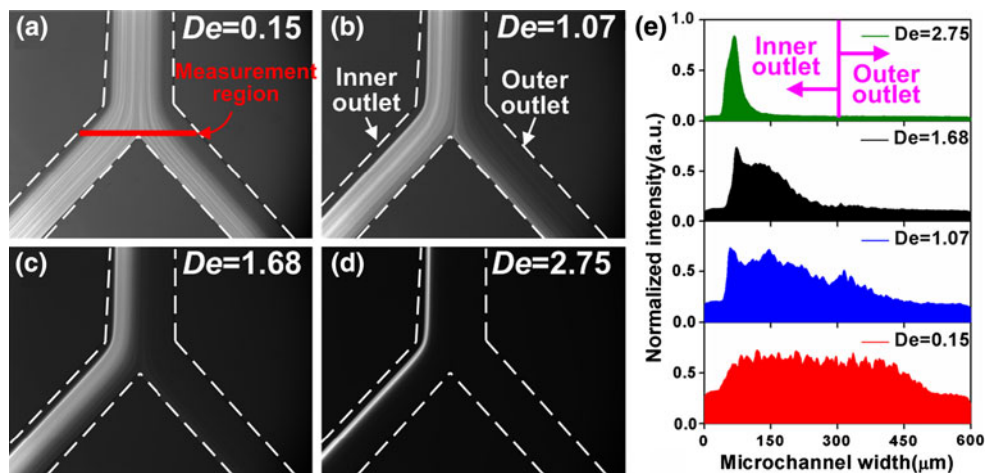


**Fig. 9** Particle filtration application based on inertial focusing. **a–d** Fluorescent stream images indicating the distribution of  $4.8 \mu\text{m}$  particles at four different flow rates ( $De = 0.15, 1.07, 1.68$  and  $2.75$ )

near specific locations. At the first loop of position one, where the particle migration length  $L = 0$  mm, distribution of  $4.8 \mu\text{m}$  particles remains uniform. As the particle migration length increases to be larger than  $11.52$  mm, particles tend to migrate towards the equilibrium positions, resulting in the emergence of a particle-free region. Finally, all the particles are well focused to the equilibrium positions, forming a single stream near the inner wall at the microchannel outlets. The width of fluorescent streams is used as a parameter to evaluate the particle focusing degree under different migration lengths. The curves in Fig. 8b describe the relationship between particle migration length ( $L$ ) and normalized fluorescent stream width. It can be found that the width of normalized fluorescent streams decreases with the increase of particle migration length ( $L$ ) under two different flow rates ( $De = 2.75$  and  $1.68$ ). Small oscillations may occur as a result of the inevitable variation of experimental parameters (i.e., concentration of the particle suspensions and size of the particles) during the whole experiment.

#### 4.5 Particle sorting and filtration applications based on inertial focusing

Based on the previous characterization of particle behavior, precise and high-throughput filtration of  $4.8 \mu\text{m}$  particles with extreme low concentration (volume concentration  $<0.005\%$ ) is achieved by using the focusing function of the spiral microchannel designed in this work. Figure 9a–d shows the distributions of  $4.8 \mu\text{m}$  particles at four different flow rates near the bifurcated outlets. The normalized fluorescent intensity distribution across the measurement region marked in Fig. 9a is shown in Fig. 9e. As can be seen from these figures, although particles at  $De = 0.15$

near the bifurcated outlets. *White dotted lines* in the figures indicate the microchannel walls. **e** Normalized fluorescent intensity distribution of  $4.8 \mu\text{m}$  particle streams in the measurement region marked in figure **a**

have begun to migrate towards the equilibrium positions, they bifurcate into the two outlets in almost equal numbers (Fig. 9a), indicating that the focusing degree is rather low at this flow rate. In consistence with the above-mentioned experimental result, the focusing degree increases along with the flow rate. As the flow rate increases to  $De = 1.68$ , more than  $90\%$  particles are collected at the inner outlet (Fig. 9c). After  $De$  is more than  $2.75$ , all particles are collected at this outlet (Fig. 9d). This method enables high-throughput filtration and concentration of various biological particles by size and can be further used for the extraction of particle-free suspension fluids, i.e., separation plasma from the whole blood sample.

The high-throughput size-based separation of  $4.8$  and  $2.1 \mu\text{m}$  particles (volume concentration  $<0.005\%$ ) is also achieved by applying the difference in their focusing states. Figure 10 shows the separation properties of mixed-particles near the outlet region. Particles are observed to remain mixed together at  $De = 3.05$  (Fig. 10a) but be separated into two overt streamlines as the flow rate increases to  $De = 5.49$  (Fig. 10b). These results are confirmed by the distributions of the normalized fluorescent intensities in the measurement region marked in Fig. 10b. In these curves (Fig. 10d), an obvious trough is found near the inner wall at  $De = 5.49$ , indicating the complete separation of these two particles. By using the fluorescence mirror unit (U-MWB2), it can be seen that the  $4.8 \mu\text{m}$  particles are well focused near the inner wall at  $De = 5.49$  (Fig. 10c). While the smaller  $2.1 \mu\text{m}$  particles are not focused to a narrow stream, they do generate double particle-free regions at this flow rate. Most importantly, the narrow stream formed by  $4.8 \mu\text{m}$  particles is exactly located in the inner wall particle-free region of  $2.1 \mu\text{m}$  particles so that complete separation of these two particles can be achieved. Using this

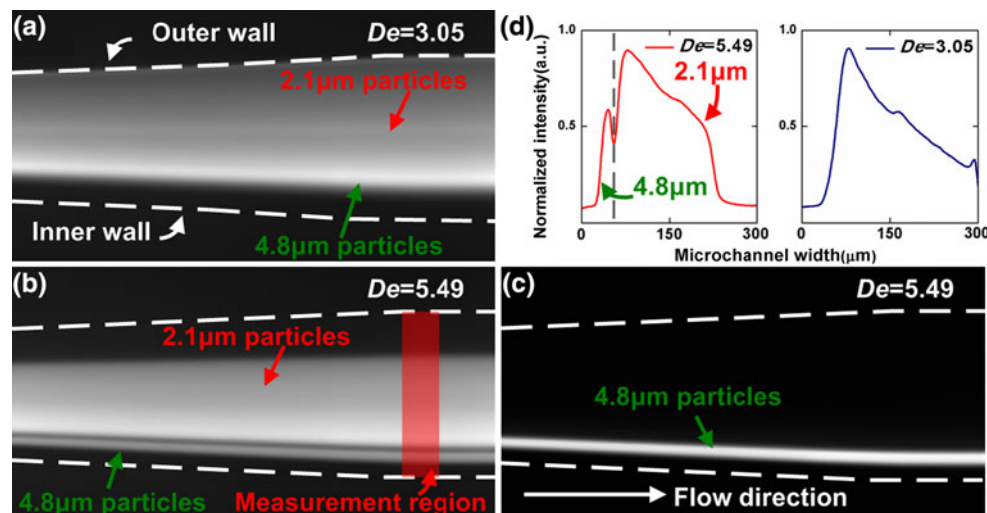


**Fig. 10** Particle sorting application based on focusing states. **a–b** Fluorescent stream images indicating the separation effects of 4.8 and 2.1  $\mu\text{m}$  particles at two different flow rates ( $De = 3.05$  and  $5.49$ ) near the outlets. **c** Fluorescent stream image captured by using the fluorescence mirror unit (U-MWB2) indicating the focusing state

separation scheme, high-throughput separation of two different-sized particles can be achieved between particles smaller and larger than the critical cutoff size ( $\sim 3.5 \mu\text{m}$  in our channel design, which is calculated with the focusing condition  $a_p/H \geq 0.07$ ). In addition to the above separation scheme, separation of multi-sized particles can also be realized in this microchannel design by varying the outlet structure. However, the principle is completely different from that for the separation of two differently sized particles as presented in this work. High-throughput separation of multi-sized particles can be achieved in virtue of the mechanism that focused particles with various sizes will equilibrate at different positions along the inner wall. To use this separation scheme, the particle sizes have to satisfy the focusing condition (i.e., the sizes of all particles need to be larger than  $\sim 3.5 \mu\text{m}$  threshold using our microchannel design).

## 5 Conclusions

In summary, a compact microfluidic device with a five-loop planar Archimedean spiral microchannel was fabricated to systematically study the inertial particle flow. The improved characterization of the focusing process or migration behavior of different-sized microparticles in the outlet region provides important insights into the design and operation of high-throughput, precise particle/cell manipulation. Quantitative analysis of these behaviors may also be useful for understanding the inertial focusing/migration mechanisms in spiral microchannels. In addition,

of 4.8  $\mu\text{m}$  particles at  $De = 5.49$ . White dotted lines in the figures indicate the microchannel walls. **d** Normalized fluorescent intensity distribution of 4.8 and 2.1  $\mu\text{m}$  particle streams in the measurement region marked in figure **b** at  $De = 3.05$  and  $5.49$

particle behaviors along the spiral microchannel were explored, which may be valuable for the optimization of microchannel structures. Furthermore, this device can be used to efficiently filter rare particles from a large-volume sample and separate particles of two different sizes according to their focusing states. Preliminary testing results using 2.1 and 4.8  $\mu\text{m}$  particles as objects show good performances. After further amelioration, this device can be developed into a powerful and high-throughput sample preparation tool for the isolation or separation of rare targets (e.g., bacteria, cancer cells) from biological or industrial samples. Furthermore, the low flow rate feature of this device enables the integrated micropump to be one of the cost-effective methods to drive sample fluids.

**Acknowledgments** This research work was supported by the Major Program of the National Natural Science Foundation of China (91023024), the National Natural Science Foundation of China (51145009), the Specialized Research Fund for the Doctoral Program of Higher Education (20110092110003), and the Jiangsu Graduate Innovative Research Program (CXZZ\_0138).

## References

- Asmolov ES (1999) The inertial lift on a spherical particle in a plane Poiseuille flow at large channel Reynolds number. *J Fluid Mech* 381:63–87
- Berger SA, Talbot L, Yao L-S (1983) Flow in curved pipes. *Annu Rev Fluid Mech* 15(1):461–512
- Bhagat AAS, Kuntaegowdanahalli SS, Papautsky I (2008a) Continuous particle separation in spiral microchannels using dean flows and differential migration. *Lab Chip* 8(11):1906–1914

- Bhagat AAS, Kuntaegowdanahalli SS, Papautsky I (2008b) Enhanced particle filtration in straight microchannels using shear-modulated inertial migration. *Phys Fluids* 20(10):101702
- Bhagat AAS, Kuntaegowdanahalli SS, Papautsky I (2009) Inertial microfluidics for continuous particle filtration and extraction. *Microfluid Nanofluid* 7(2):217–226
- Bhagat AAS, Kuntaegowdanahalli SS, Kaval N, Seliskar CJ, Papautsky I (2010) Inertial microfluidics for sheath-less high-throughput flow cytometry. *Biomed Microdevices* 12(2):187–195
- Choi Y-S, Lee S-J (2010) Holographic analysis of three-dimensional inertial migration of spherical particles in micro-scale pipe flow. *Microfluid Nanofluid* 9(4):819–829
- Choi Y-S, Seo K-W, Lee S-J (2011) Lateral and cross-lateral focusing of spherical particles in a square microchannel. *Lab Chip* 11(3):460–465
- Di Carlo D, Irimia D, Tompkins RG, Toner M (2007) Continuous inertial focusing, ordering, and separation of particles in microchannels. *Proc Natl Acad Sci USA* 104(48):18892–18897
- Di Carlo D, Edd JF, Irimia D, Tompkins RG, Toner M (2008) Equilibrium separation and filtration of particles using differential inertial focusing. *Anal Chem* 80(6):2204–2211
- Edd JF, Di Carlo D, Humphry KJ, Koster S, Irimia D, Weitz DA, Toner M (2008) Controlled encapsulation of single-cells into monodisperse picolitre drops. *Lab Chip* 8(8):1262–1264
- Gossett DR, Di Carlo D (2009) Particle focusing mechanisms in curving confined flows. *Anal Chem* 81(20):8459–8465
- Kim YW, Yoo JY (2008) The lateral migration of neutrally-buoyant spheres transported through square microchannels. *J Micromech Microeng* 18(6):065015
- Kuntaegowdanahalli SS, Bhagat AAS, Kumar G, Papautsky I (2009) Inertial microfluidics for continuous particle separation in spiral microchannels. *Lab Chip* 9(20):2973–2980
- Lee MG, Choi S, Kim H-J, Lim HK, Kim J-H, Huh N, Park J-K (2011) Inertial blood plasma separation in a contraction–expansion array microchannel. *Appl Phys Lett* 98(25):253702
- Mach AJ, Kim JH, Arshi A, Hur SC, Di Carlo D (2011) Automated cellular sample preparation using a Centrifuge-on-a-Chip. *Lab Chip* 11(17):2827–2834
- Ookawara S, Higashi R, Street D, Ogawa K (2004) Feasibility study on concentration of slurry and classification of contained particles by microchannel. *Chem Eng J* 101(1–3):171–178
- Russom A, Gupta AK, Nagrath S, Di Carlo D, Edd JF, Toner M (2009) Differential inertial focusing of particles in curved low-aspect-ratio microchannels. *New J Phys* 11(7):075025
- Seo J, Lean MH, Kole A (2007a) Membrane-free microfiltration by asymmetric inertial migration. *Appl Phys Lett* 91(3):033901
- Seo J, Lean MH, Kole A (2007b) Membraneless microseparation by asymmetry in curvilinear laminar flows. *J Chromatogr A* 1162(2):126–131
- Sim TS, Kwon K, Park JC, Lee J-G, Jung H-I (2011) Multistage-multiorifice flow fractionation (MS-MOFF): continuous size-based separation of microspheres using multiple series of contraction/expansion microchannels. *Lab Chip* 11(1):93–99
- Squires TM, Quake SR (2005) Microfluidics: fluid physics at the nanoliter scale. *Rev Mod Phys* 77(3):977–1026
- Sudarsan AP, Ugaz VM (2006a) Fluid mixing in planar spiral microchannels. *Lab Chip* 6(1):74–82
- Sudarsan AP, Ugaz VM (2006b) Multivortex micromixing. *Proc Natl Acad Sci USA* 103(19):7228–7233
- Wang J, Zhan Y, Ugaz VM, Lu C (2010) Vortex-assisted DNA delivery. *Lab Chip* 10(16):2057–2061
- Xuan X, Zhu J, Church C (2010) Particle focusing in microfluidic devices. *Microfluid Nanofluid* 9(1):1–16
- Yoon DH, Ha JB, Bahk YK, Arakawa T, Shoji S, Go JS (2009) Size-selective separation of micro beads by utilizing secondary flow in a curved rectangular microchannel. *Lab Chip* 9(1):87–90